Biomolecule-assisted route for shape-controlled synthesis of single-crystalline $MnWO_4$ nanoparticles and spontaneous assembly of polypeptide-stabilized mesocrystal microspheres†

Thanh-Dinh Nguyen, Driss Mrabet, Thi-Thuy-Duong Vu, Cao-Thang Dinh and Trong-On Do*

Received 14th April 2010, Accepted 2nd October 2010
DOI: 10.1039/c0ce00091d

Single-crystalline mixed metal oxide nanoparticles and 3D hierarchical mesocrystal microspheres of $MnWO_4$ have been synthesized on a large scale by a facile single-step hydrothermal method using $Mn(NO_3)_2$ and Na_2WO_4 precursors, and capping bifunctional amino acid biomolecules with different alkyl chain lengths, and water or water/ethylene glycol medium. The resulting single-crystalline $MnWO_4$ nanoparticles with different uniform shapes including bar, rod, square, quasi-sphere, sphere, hexagonal crystals were obtained by tuning the synthetic conditions such as the concentration and the alkyl chain length of amino acids, pH, and reaction temperature. By decreasing the Mn^{2+} and WO_4^{2-} precursor monomer concentration from 0.0150 to 0.0076 M in aqueous media, polypeptide-stabilized $MnWO_4$ mesocrystal hierarchical microspheres were achieved, due to the spontaneous-assembly of primary nanoparticles through the back-bone–back-bone intermolecular hydrogen bonding interactions of polypeptide chains. Nanoplatelet-based microapples with two holes on their poles were also obtained under the same synthetic conditions for the microspheres, except that the use of water/ethylene glycol (10 : 30 mL) instead of water medium. The photoluminescence (PL) results revealed that the PL emission intensity of the $MnWO_4$ nanobars is higher than that of the self-assembled $MnWO_4$ microspheres. This green chemistry method is simple and highly reproducible, using inexpensive reagents, and water as reaction solvent. The uniform $MnWO_4$ nanorods with the control of aspect ratio (length/width) can be produced in a large quantity as much as 16 g in a single preparation. The current approach is quite general and able to be extended to a variety of other well-defined metal oxide and mixed oxide nanomaterials with controlled shapes.

1. Introduction

Over the past decade, shape-controlled syntheses of mixed metal oxide nanoparticles have become one of the essential topics in nanomaterials science, since their unique properties are generally not available in single metal oxide nanoparticles.[1] Mixed metal oxide nanoparticles with different shapes have therefore gained much attention in the fields of catalysis, electronics, optics, sensors, biology, magnetism, luminescence, and drug delivery.[2,3] The shape of the nanomaterials is an important factor that dictates their physicochemical properties because the number of active atoms located at the edges/corners and exposed facets of crystals.[4,5] In addition, the self-assembly of tailored nano-building units into three-dimensional (3D) mixed metal oxide microarchitectures has recently received considerable interest.[6,7] Many novel and fascinating properties of these materials are predicted depending not only on the complex morphology but also on the order degree of single-crystalline nanoparticles in microarchitectures.[8] For example, the photoluminescence (PL) from single-disk spherical superparticles of CdSe/CdS nanorod building blocks did not have a significant linear polarization, but individual bilayer spherical superparticles exhibited strongly linearly polarized emissions.[9] Therefore, exquisite shape and control of both uniform single-crystalline mixed oxide nanoparticles and self-assembled hierarchical microarchitectures are highly desirable for tailoring their specific properties and are also required for high performance in many applications.

Manganese tungstate ($MnWO_4$) is one of the most promising mixed metal oxide nanomaterials, which exhibits high sensitivity to humidity change and unique magnetic property.[10–13] Hence, it has attracted considerable research interest for potential applications such as photocatalysts, humidity sensors, optical fibers, photoluminescence and scintillator materials.[14–18] These exciting applications originate from its electrical conductivity property, which depends on the shape of the products.[19–21] Therefore, several efforts have been devoted to the synthesis of $MnWO_4$ nanoparticles and especially focused on the shape and dimensional control. For instance, a general hydrothermal route for the synthesis of single-crystalline tungstate AWO_4 (A = Mn, Fe, Zn) nanorods/nanowires with wolframite structures was reported by Qian *et al.*[22] Thongtem *et al.*[23] prepared $MnWO_4$ nanostructures through a cyclin microwave-assisted spay method. Yu *et al.*[24] hydrothermally fabricated 3D urchin-like $MnWO_4$ microspheres assembled by nanorods with the aid of cationic surfactant cetyltrimethyl ammonium bromide (CTAB). Our group has recently developed some new routes for the synthesis of shape-controlled

Department of Chemical Engineering, Laval University, Quebec, Canada G1K 7P4. E-mail: Trong-On.Do@gch.ulaval.ca; Fax: +1 (418) 656-5993; Tel: +1 (418) 656-3774

† Electronic supplementary information (ESI) available: Additional SEM/TEM, EDS, XPS, FTIR results of $MnWO_4$ nano- and microstructures. See DOI: 10.1039/c0ce00091d

oxide and mixed oxide nanocrystals using surfactant-stabilized precursors.[25–29] So far, recent efforts have been focused on the assembled restructuring of the individual nanocomponents into microspheres through the interaction of functionalized nanoparticles. Generally, two "bottom-up" approaches for the hierarchical microarchitectures have been widely used: (i) "two-step" synthesis has mostly employed the replacement of hydrophobic ligands by hydrophilic ones or *in situ* grow a hydrophilic shell on a pre-synthesized nanoparticles in emulsions or ionic liquids.[30,31] However, the addition of a template to the reaction system involves a complicated process and may result in impurities due to the incomplete removal of the template. (ii) "One-step" one has carefully examined by various reaction factors to organize artificial nano-building blocks into 3D architectures with the aid of the surface functional groups.[32,33] The latter method thus seems to be more attractive and promising, owing to its higher yield and simplicity. To our best knowledge, no aqueous-based amino acid-assisted method for "one-step" synthesis of single-crystalline $MnWO_4$ nanoparticles with diversely controllable shapes and architectures in terms of low cost and potential for large-scale production has been reported.

In the present study, we report a new approach for the aqueous-phase synthesis of uniform single-crystalline $MnWO_4$ nanoparticles with controlled shape and the self-assembled mesocrystal microspheres/microapples with high yield using $Mn(NO_3)_2$ and Na_2WO_4 as precursors and bifunctional amino acid biomolecules as capping agent. This work consists of two parts. In the first part, we focus on the large-scale synthesis of single-crystalline $MnWO_4$ nanoparticles with various shapes by tuning the concentration and the alkyl chain length of amino acid surfactants, pH, and reaction temperature. Secondly, we describe a "single-step" synthesis of 3D hierarchical $MnWO_4$ mesocrystal microspheres and micro like-apples from the spontaneous assembly of individual nanoparticles by adjusting the precursor monomer concentration in water or in water/ethylene glycol medium. The possible mechanisms for the formation of single-crystalline $MnWO_4$ nanoparticles and their self-assembled microspheres are proposed. The optical properties of these $MnWO_4$ samples with various morphologies are also reported.

2. Experimental

Chemicals

All chemicals were used as received without further purification. Manganese(II) nitrate tetrahydrate ($Mn(NO_3)_2{\cdot}4H_2O$, 99%), sodium tungstate dihydrate ($Na_2WO_4{\cdot}2H_2O$, 99.9%), 5-aminovaleric acid ($HOOCC_4H_8NH_2$, or AVA, 97%), 6-aminohexanoic acid ($HOOCC_5H_{10}NH_2$, or AHA, 70%), 2-aminononanoic acid ($HOOCC_9H_{19}NH_2$ or ANA, 90%), hexamethylenediamine ($NH_2(CH_2)_6NH_2$, 98%), were purchased from Sigma–Aldrich. Nitric acid (HNO_3, 63%) and ethylene glycol ($HOCH_2CH_2OH$, 99.8%) are of analytical grade and purchased from Reagent ACS.

(i) Synthesis of $MnWO_4$ nanoparticles with bar, rod, square, quasi-sphere, sphere and hexagonal shapes

$Mn(NO_3)_2{\cdot}6H_2O$ (0.61 mmol, 0.153 g) and 6-aminohexanoic acid (1.22 mmol, 0.16 g) were dissolved in 20 mL of distilled water. 20 mL of an aqueous $Na_2WO_4{\cdot}2H_2O$ 30.5 mM solution was added to the above aqueous solution under magnetic stirring for about 10 min at room temperature. A white coloured amorphous $MnWO_4$ precipitate appeared immediately because of the combination of Mn^{2+} cations and WO_4^{2-} anions. The resulting reaction mixture (40 mL) was transferred to a Teflon-lined stainless steel autoclave of 70 mL capacity and treated at desired temperature in the range of 180 °C for 20 h, and then cooled naturally to room temperature. The obtained product was filtered out, washed several times by ethanol, and dried at 60 °C for 2 h. The $MnWO_4$ nanoparticles with various shapes (including bar, rod, square, quasi-sphere, sphere, hexagonal) have been controlled by varying reaction parameters such as concentration of 6-aminohexanoic acid (0.031–0.915 M), alkyl chain length of amino acid surfactants (*e.g.*, 5-aminovaleric acid, 6-aminohexanoic acid, 2-aminononanoic acid), pH of synthesis solution (ranging from 9 to 6, the pH value was adjusted to a desired pH value using 1 mol L^{-1} HNO_3 solution), and reaction temperature (180–220 °C).

(ii) Synthesis of self-assembled $MnWO_4$ microspheres and micro-like apples

$MnWO_4$ hierarchical microspheres were produced in water medium when the precursor monomer concentration of $Mn(NO_3)_2$ and Na_2WO_4 salts in bulk solution decreased from 0.0150 to 0.0076 M, while keeping the other synthesis conditions unchanged ($[Mn^{2+}] = [WO_4^{2-}] = 1:1$, 0.031 M of 6-aminohexanoic acid, pH = 9, 180 °C, 20 h). The nanoplatelet-based microapples obtained under the same reaction conditions for the synthesis of microspheres, except that water–ethylene glycol (10 : 30 mL) medium was used instead of distilled water (100%).

Characterization

X-Ray diffraction (XRD) data were recorded on a Bruker SMART APEXII X-ray diffractometer, using Cu-Kα radiation ($\lambda = 1.5418$ Å). Transmission electron microscope (TEM) images and selected area electron diffraction (SAED) patterns were obtained on a JEOL JEM 1230 operated at 120 kV. High-resolution TEM images were taken on a JEOL field-emission transmission electron microscope (2100F) operated at 200 kV. The samples were prepared by placing a drop of an anhydrous ethanol dispersion of product onto a 200 mesh carbon coated copper grid and immediately evaporated at ambient temperature. Scanning electron microscope (SEM) images and elemental dispersive spectrum (EDS) analyses were obtained from a JEOL 6360 instrument working at 3 kV. XPS measurement was carried out in an ion-pumped chamber (evacuated to 10^{-9} Torr) of a photoelectron spectrometer (Kratos Axis-Ultra) equipped with a focused X-ray source (Al-Kα, $hv = 1486.6$ eV). The binding energy of the samples was calibrated by setting the C 1s peak to 285 eV. The peaks were deconvoluted by means of a standard CasaXPS software (v 2.3.13; product of CasaXPS Software Ltd., USA) to resolve the separate constituents after background subtraction. FTIR spectrum was measured with FTS 45 infrared spectrophotometer with the KBr pellet technique. Thermogravimetric analysis (TGA) was carried out with a heating rate of 10 °C min^{-1}, under an air flux up to 600 °C using a Perkin-Elmer

TGA thermogravimetric analyzer. The specific surface area was calculated from the linear part of the Brunauer–Emmett–Teller equation ($P/P_0 \approx 0.05$–0.2). The pore diameter distribution was obtained from analysis of the desorption branch of the isotherms using the Barrett–Joyner–Halenda model. UV–vis spectra were recorded for the as-synthesized $MnWO_4$ nanobars and microspheres in distilled water on a Cary 300 Bio UV-visible spectrophotometer, and distilled water was used as a blank. The room temperature photoluminescence spectrum was measured on an optical spectrum analyzer (ANDO AQ6317, Japan).

3. Results and discussion

Uniform single-crystalline nanoparticles and 3D hierarchical mesocrystal microspheres of $MnWO_4$ were synthesized by a simple "one-step" hydrothermal method using $Mn(NO_4)_2$ and Na_2WO_4 as starting materials, 6-aminohexanoic acid as capping agent, and distilled water or water–ethylene glycol as synthesis medium at 180–220 °C for 20 h. Bifunctional amino acid molecules, which were used in this study, are composed of an alkyl chain (*e.g.*, C_5, C_6 or C_{10}) and two head ends of $–NH_2$/–COOH groups. Table 1 summarizes the synthesis conditions and various morphologies of the as-prepared $MnWO_4$ samples *via* bifunctional amino acid-assisted hydrothermal process. In the early stage of the synthesis, $MnWO_4$ nuclei were formed by the combination of Mn^{2+} cations and WO_4^{2-} anions. This stage is followed by the crystal growth process. The nanoparticle products were capped by the amino head groups of amino acid biomolecules and their surface become hydrophilic owing to other end of the uncoordinated carboxylic groups (see Scheme 1). Due to the hydrophilic surface character, the final products can be suspended in water medium. Various shapes of particle products can be controlled depending on synthetic conditions (see Table 1). The influence of synthetic conditions on shape was systematically studied by altering the concentration of reaction reagents, alkyl chain length of amino acid surfactant, pH of solution, and reaction temperature. Different precursor monomer concentrations ranging from 0.0120 to 0.0076 M in water or water/ethylene glycol medium were studied to determine the optimal conditions for the formation of polypeptide-stabilized $MnWO_4$ mesocrystal microspheres and micro-like apples (see Scheme 2).

Using 6-aminohexanoic acid (AHA) as a capping agent, the experimental results revealed that the AHA concentration in the aqueous solution plays an important role in tuning the lengths and aspect ratios (length/width) of $MnWO_4$ nanoparticles. Fig. 1 shows TEM/HRTEM images of four representative samples synthesized under the same synthesis conditions (*e.g.*, 0.015 M of $Mn(NO_3)_2$, 0.015 M of Na_2WO_4, Mn : W molar ratio = 1 : 1, pH = 9, 180 °C for 20 h), however, only the 6-aminohexanoic acid concentration in the reaction solution was changed from low to high; for example, from 0.031 to 0.305, 0.610, 0.915 M, corresponding to the AHA/(Mn + W) molar ratio ranging from 2 : 1 to 10 : 1, 20 : 1, 30 : 1. When the AHA/(Mn + W) molar ratio was 2 : 1, uniform single-crystalline nanobars (short rod) with an average diameter of 25 nm, a length of 50 nm, and an aspect ratio of 2.0 were obtained (Fig. 1a). They were slightly truncated at the corners and their surface presented without any dislocation and stacking fault; however, some defects as pinholes were found. Fig. 1b shows high-resolution TEM images with different scales of a $MnWO_4$ nanobar with the aspect ratio of 2.0, suggesting that the nanobar is single crystal with an interplanar spacing of 0.30 nm, which corresponds to the separation between the (200) lattice planes of monoclinic $MnWO_4$.[34] The side surfaces of the nanobar were bounded by (100) plane. The ends of the nanobar were enclosed by the (021) plane. This single-crystalline nanobar shows resolvable planes corresponding to the [100] and [021] directions, as illustrated in the inset of Fig. 1b. The (100) planes are oriented parallel to the nanobars' growth axis, suggesting that the growth direction of the single-crystalline nanobar occurs preferentially along the [100] direction (*c* axis). As a result, a strong (100) diffraction peak in the XRD pattern was observed (see below). A selected area electron diffraction (SAED) pattern (Fig. 1c) taken from a single nanobar (inset of Fig. 1b) also confirms the preferential [100]-oriented growth of a monoclinic $MnWO_4$ single-crystal structure. Further, an increase of the molar ratio to 10 : 1, the shape evolution of nanobar into nanorod with the average length elongated from 50 to 100 nm was yielded, while the diameter of ~25 nm remained almost unchanged (Fig. 1d). When the molar ratio was increased from 10 : 1 to 20 : 1, the average length of nanorod increased significantly from 100 to 150 nm and their diameter was still unchanged (Fig. 1e). Eventually, as this molar ratio was increased further to 30 : 1, the length of 25 nm × 150 nm-sized nanorods was still maintained (Fig. 1f). Further, bar-shaped $MnWO_4$ nanocrystals

Table 1 Synthesis conditions and morphologies of the monoclinic $MnWO_4$ nano- and microstructures *via* amino acid-assisted hydrothermal process[a]

Sample	Cation precursor/M	Anion precursor/M	Solvent/mL	Amino acid/M	pH	*T*/°C	Size and shape/nm
1	0.015, $Mn(NO_3)_2$	0.015, Na_2WO_4	H_2O	0.031 AHA	9	180	25 × 50 nm, bar
2	0.015, $Mn(NO_3)_2$	0.015, Na_2WO_4	H_2O	0.305 AHA	9	180	25 × 100 nm, rod
3	0.015, $Mn(NO_3)_2$	0.015, Na_2WO_4	H_2O	0.610 AHA	9	180	25 × 150 nm, rod
4	0.015, $Mn(NO_3)_2$	0.015, Na_2WO_4	H_2O	0.031 AHA	6	180	25 nm, square
5	0.015, $Mn(NO_3)_2$	0.015, Na_2WO_4	H_2O	0.031 AHA	6	200	18 nm, quasi-sphere
6	0.015, $Mn(NO_3)_2$	0.015, Na_2WO_4	H_2O	0.031 AHA	6	220	18 nm, sphere
7	0.015, $Mn(NO_3)_2$	0.015, Na_2WO_4	H_2O	0.031 AVA	9	180	25 × 50 nm, bar
8	0.015, $Mn(NO_3)_2$	0.015, Na_2WO_4	H_2O	0.031 ANA	9	180	18 nm, hexagonal
9	0.0076, $Mn(NO_3)_2$	0.0076, Na_2WO_4	H_2O	0.031 AHA	9	180	7 μm, microsphere
10	0.0076, $Mn(NO_3)_2$	0.0076, Na_2WO_4	water–EG	0.031 AHA	9	180	3 μm, microapple

[a] All samples were synthesized by hydrothermal process for 20 h; 5-aminovaleric acid (AVA), 6-aminohexanoic acid (AHA), 2-amininononanoic acid (ANA), water–ethylene glycol (10 : 30 mL).

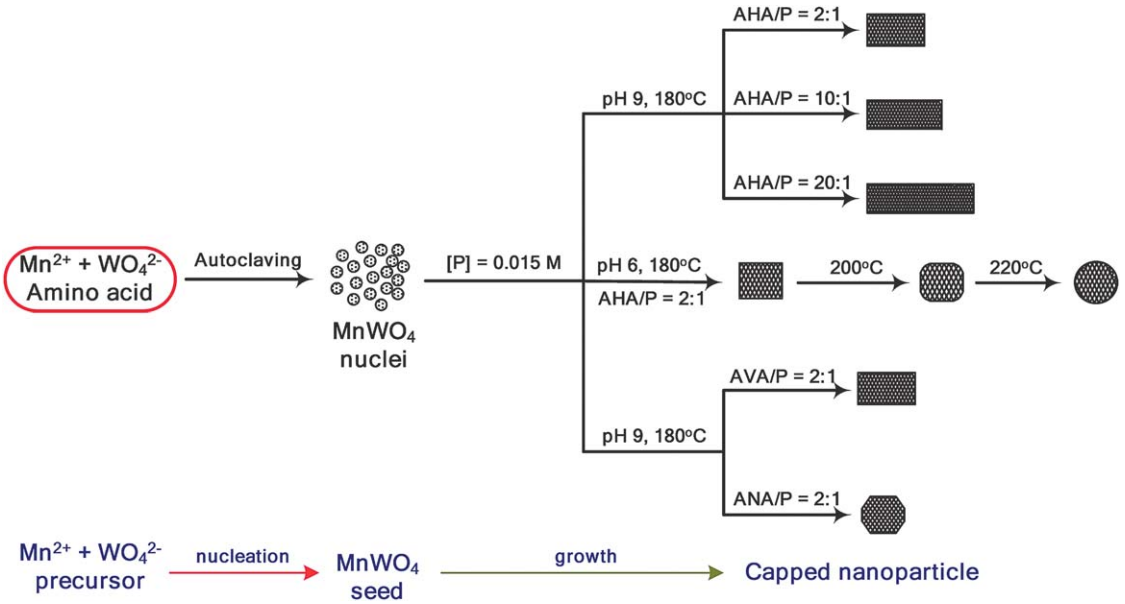

Scheme 1 Schematic illustration of the overall formation and various shape control of the monodisperse $MnWO_4$ nanoparticles using high precursor monomer concentration (0.015 M).

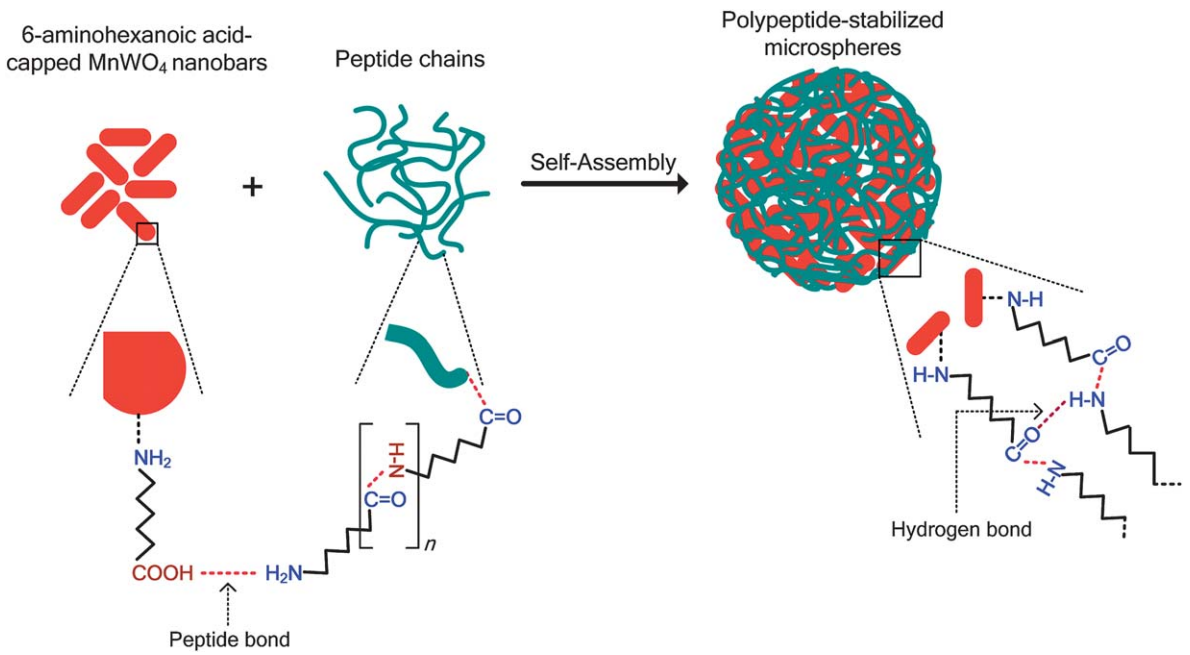

Scheme 2 A possible proposed mechanism for the construction of 3D hierarchical $MnWO_4$ microspheres from spontaneous-assembly of nanobars using low precursor monomer concentration (0.0076 M).

were still produced but no well-shape when the synthetic reaction was performed at lower temperature (140–160 °C), indicating that a thermodynamic equilibrium of nanobars was being established at a wide range of the temperature (ESI, Fig. S1).†

The elongation of nanoparticles from 25 nm × 50 nm-sized nanobar to 25 nm × 150 nm-sized nanorods with increasing 6-aminohexanoic acid (AHA) concentration from 0.031 to 0.610 M was clearly observed. The general trend is sketched in Fig. 1g. This observation indicates that the high surfactant concentration (0.610 M) favours the over growth of an anisotropic $MnWO_4$ structure and a long nanorod (high aspect ratio) was obtained. However, with higher surfactant concentrations (≥0.915 M), no significant change in the aspect ratio was observed suggesting that the equilibrium of growth kinetics could be established at this surfactant concentration. These experimental results suggest that the (021) faces of nanocrystals were selectively adsorbed and stabilized by AHA molecules, while the (100) faces were uncovered. The crystal grew anisotropically along the [100] direction due to their higher surface energies resulting in the nanorod product. Because AHA adsorbed onto only specific (021) faces, the nanorods with high

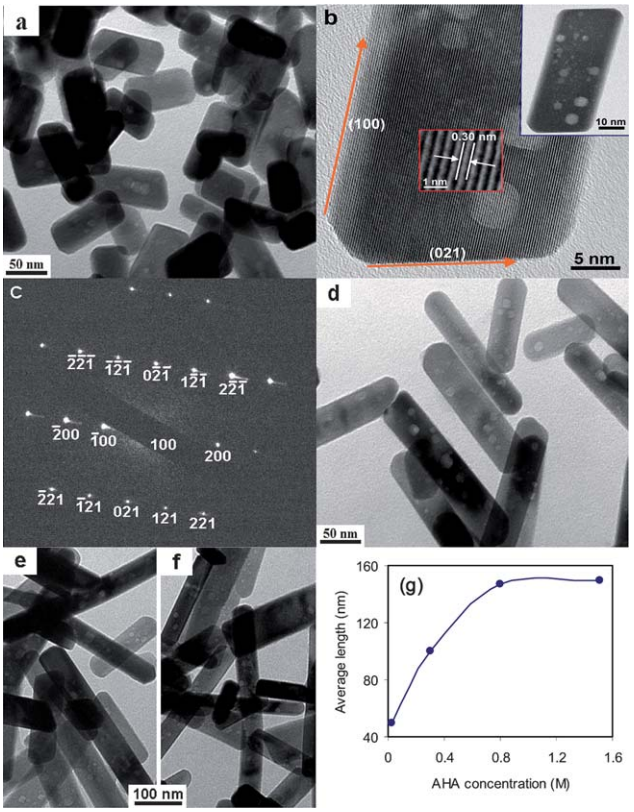

Fig. 1 TEM images of the $MnWO_4$ nanoparticles synthesized from an aqueous solution of 0.015 M $Mn(NO_3)_2$ and 0.015 M Na_2WO_4, pH = 9, 180 °C for 20 h, using the different 6-aminohexanoic acid/(Mn + W) molar ratios (AHA/P): (a) 25 nm × 50 nm nanobars, AHA/P = 2 : 1; (b) HRTEM image of an individual nanobar; (c) SAED pattern of a single bar taking along [100] zone axis; (d) 25 nm × 100 nm nanorods, AHA/P = 10 : 1; (e) 25 nm × 150 nm nanorods, AHA/P = 20 : 1; (f) 25 nm × 150 nm nanorods, AHA/P = 30 : 1; (g) Correlation plot showing the relationship of 6-aminohexanoic acid concentration and average length of $MnWO_4$ nanorods.

aspect ratios produced at high AHA concentration could be due to the oriented attachment of nanocrystals predominantly during the synthesis.[35] To study the effect of the pH of synthesis solution as well as the reaction temperature on shape of the $MnWO_4$ products, a series of experiments was carried out under the same reaction conditions, except that either the pH of solution or the reaction temperature changed. As seen in Fig. 1a, for sample 1 in Table 1, at 180 °C, with pH of 9, 25 nm × 50 nm nanobars were obtained. Under the same synthesis conditions, however, the pH of initial solution was 6 instead of 9. The pH of 6 in the initial solution was adjusted by using 1 M HNO_3 solution. $MnWO_4$ square-like nanosheets with the particle size of ~25 nm were produced (Fig. 2a). This indicates the change of shape from the nanobars to the square-like nanosheets by only decreasing the pH of solution from 9 to 6. The pH change in the reaction solution could influence the binding and selective adsorption of the surfactant molecules on the particle surface leading to the shape change of the products. In this case, the shape change could be due to the protonation/deprotonation and consequently a decrease of selective adsorption of 6-aminohexanoic acid molecules (AHA) to crystal faces with the pH change from 9 to 6. Fig. 2 also shows

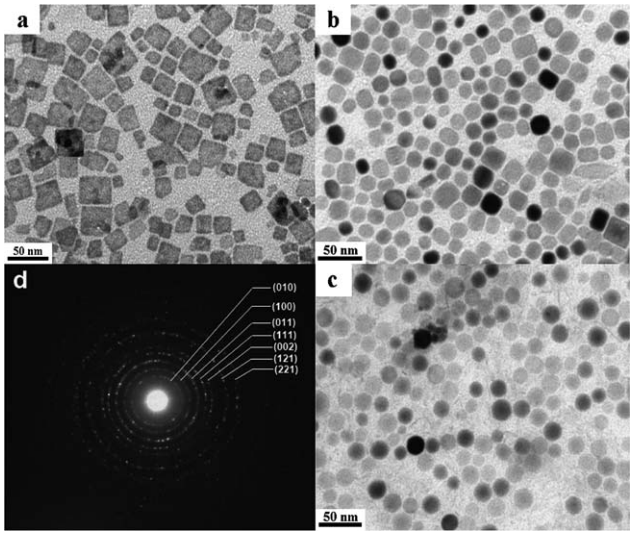

Fig. 2 TEM images of the $MnWO_4$ nanoparticles synthesized from an aqueous solution of 0.015 M of $Mn(NO_3)_2$ and 0.015 M of Na_2WO_4, AHA/(Mn + W) molar ratio of 2 : 1, pH = 6, at the different reaction temperatures: (a) 18 nm square-like nanosheets, 180 °C; (b) 18 nm quasi-nanospheres, 200 °C; (c) 18 nm nanospheres, 220 °C; (d) SAED pattern of a single sphere in panel c, showing the single-crystal nature.

TEM images of the $MnWO_4$ nanoparticles synthesized with the pH of 6 instead of 9 for 20 h at different reaction temperatures: 180, 200, 220 °C, and keeping the other conditions unchanged ($[Mn^{2+}] = [WO_4^{2-}] = 0.015$ M, AHA/(Mn + W) = 2 : 1).

Under these synthetic conditions (with pH = 6) as increasing the temperature from 180 to 200 °C, 18 nm-sized quasi-nanospheres were produced (Fig. 2b). At the reaction temperature of 220 °C, nanospheres were found instead of quasi-nanospheres (Fig. 2c). SAED pattern of a single sphere, as seen in Fig. 2d, exhibits strong ring patterns assigned to (100), (011), (111), (002), (102) planes, corresponding to a pure monoclinic phase of $MnWO_4$, and proves a single-crystal structure of the nanospheres, which is consistent with the XRD data (see below). These results indicate that for the pH of 6, increasing reaction temperature from 180 to 220 °C, the shape of $MnWO_4$ nanoparticles was changed from square into sphere, while preserving their particle size and monoclinic structure. This shape change could be explained by the Wuff facets theory.[36,37] According to this theory, the growth rate of a crystal facet depends exponentially on the surface energy. High-energy facets thus grow more quickly than others and they were minimized surface energies during growth.[38]

Because no monomer precursors were added during the synthesis, at the relatively low reaction temperature (*e.g.*, 180 °C), the $MnWO_4$ nanosquares were formed in the anisotropic growth of high-energy crystal faces owing to high precursor monomer concentration in bulk solution. At higher synthesis temperature (*e.g.*, 200–220 °C), the shape change of the nanoparticles from square to quasi-sphere and final to uniform sphere may result in the insufficient coverage of AHA molecules toward crystal faces owing to weak interactions between AHA and nanoparticles. The depletion of remaining precursor monomer concentration in bulk solution to a level lower than that required for a given anisotropic shape. Consequently, the

monomers of the dissolved crystals at higher energy faces could move thermodynamically to the lower energy faces to minimize the surface energies. As a result, the corners and tips of the square-shaped $MnWO_4$ nanoparticles were "rounded", which leads to the formation of stable nanospheres with a minimum face energy.

Fig. 3 shows XRD patterns of the $MnWO_4$ samples of 25 nm × 50 nm nanobars and 18 nm nanospheres. All the diffraction peaks of both samples are well indexed to monoclinic $MnWO_4$ phase with lattice parameters of $a = 4.819$ Å, $b = 5.771$ Å, $c = 5.005$ Å, which are comparable with reported database values of $a = 4.829$ Å, $b = 5.759$ Å, $c = 4.998$ Å for bulk $MnWO_4$ (JCPDS File no. 13-0434).[39] The broadening and intense diffraction peaks indicate the small particle size and high crystallinity of the as-synthesized products. An average particle size of nanospheres estimated from the broadening (111) peaks using the Debye–Scherrer equation is about 16.5 nm, which is in agreement with the particle size observed from TEM images. No other phases of either single manganese oxides or tungsten oxides were detected in the $MnWO_4$ nanoparticles indicating that a pure monoclinic $MnWO_4$ phase obtained by this synthetic approach. It is observed that the intensity of the diffraction peak from (100) plane of the nanobars is stronger than that of the nanospheres. This also indicates a growth orientation of the (100) plane in a single-crystalline $MnWO_4$ nanobar, which is consistent with the HRTEM analysis.

Furthermore, to gain further insights into the steric effect of the capping ligands on the shape of $MnWO_4$ nanoparticles, two additional amino acid surfactants with different alkyl chain lengths: 5-aminovaleric acid (AVA, C_5) and 2 aminononanoic acid (ANA, C_{10}) were employed, compared to 6-aminohexanoic acid (AHA, C_6). TEM images of these samples shown in Fig. 4 indicate that when using 5-aminovaleric acid (C_5) instead of 6-aminohexanoic acid (C_6), no significant change in the shape of nanobars (25 nm × 50 nm) was observed (Fig. 4a and Fig. 1a). However, using amino acid with a longer alkyl chain length, *e.g.*, 2-aminononanoic acid (C_{10}), 18 nm-sized $MnWO_4$ nanohexagons were produced (Fig. 4b). A representative TEM image of this sample also exhibits a self-assembled 2D array of

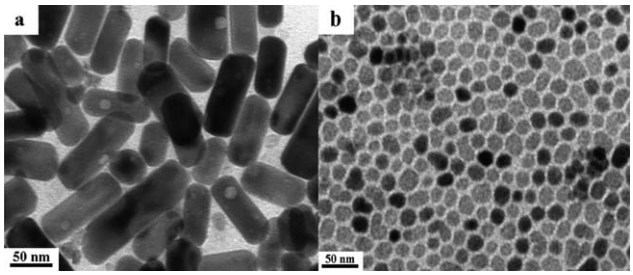

Fig. 4 TEM images of the $MnWO_4$ nanoparticles synthesized using the different alkyl chain lengths of amino acids: (a) 25 nm × 50 nm nanobars, 5-aminovaleric acid (C_5); (b) 18 nm nanohexagons, 2-aminononanoic acid (C_{10}).

nanohexagons with a nearest-neighbour spacing of ~2 nm. It can be concluded that the increase of alkyl chain length of amino acid surfactant led to the change of shape: from anisotropic (nanobar) into isotropic nanocrystal (nanosphere/nanohexagon). This is also consistent with our previous report for the synthesis of vanadium oxide nanocrystals that longer alkyl chain lengths generated smaller particles owing to the slower nucleation and growth rate.[40]

The chemical composition and oxidation state on the surface of 6-aminohexanoic acid-capped manganese tungstate nanobars (sample 1 in Table 1) were analysed by the XPS technique. The survey XPS spectrum of 25 nm × 50 nm $MnWO_4$ nanobars shows the presence of Mn 2p, W 4f, O 1s, N 1s, C 1s (ESI, Fig. S2a).† Elemental dispersive spectrum (EDS) analysis of this sample (ESI, Fig. S2b)† also exhibits the presence of Mn, W, O. The Mn : W molar ratio determined from both techniques was close to 1 : 1. Fig. 5 shows high-resolution Mn 2p and W 4f XPS spectra of this sample. For the Mn 2p XPS spectrum (Fig. 5a), two Mn $2p_{3/2}$ and Mn $2p_{1/2}$ peaks at 640.5–650.0 eV and 642.8–653.7 eV, respectively, are similar to those of bulk MnO,[41] corresponding to the oxidation state of Mn^{2+}. For the W 4f XPS spectrum (Fig. 5b), W $4f_{7/2}$ and W $4f_{5/2}$ peaks at 35.4 and 37.5 eV, respectively, were assigned to the oxidation state of W^{6+}.[42] The O 1s XPS spectrum (ESI, Fig. S3) is composed of two peaks at 530.0 and 531.8 eV, which can be assigned to Mn–O–W bond in

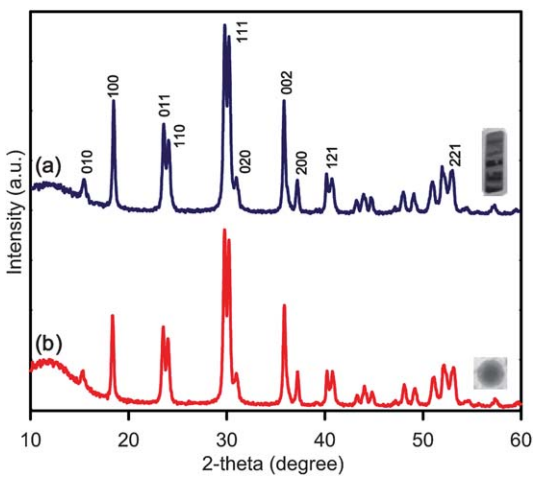

Fig. 3 XRD patterns of the as-synthesized $MnWO_4$ samples: (a) nanobars (sample 1) and (b) nanospheres (sample 6 in Table 1).

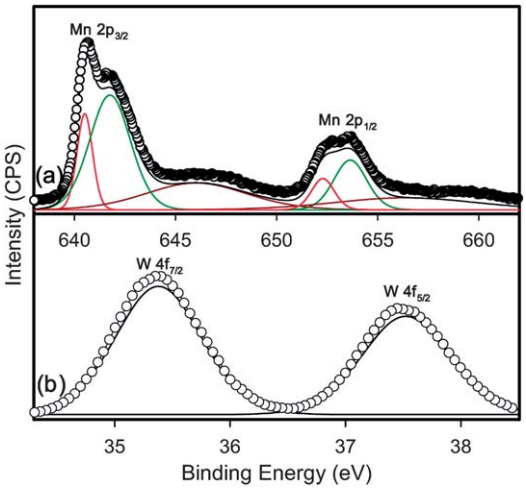

Fig. 5 High-resolution (a) Mn 2p and (b) W 4f XPS spectra of 6-aminohexanoic acid-capped $MnWO_4$ nanobars (sample 1 in Table 1).

$MnWO_4$ and O–C bond in 6-aminohexanoic acid, respectively.[43,44] This suggests that the stoichiometric ratio is close to $MnWO_4$ on the nanobar surface. The N 1s and C 1s XPS spectra of this sample shown in Fig. S4† indicate that 6-aminohexanoic acid molecules bound on the $MnWO_4$ nanobar surface. The N 1s region (ESI, Fig. S4a)† contains a main peak at 399.8 eV, which was assigned to nitrogen in $–NH_2$ group.[45] The C 1s region (ESI, Fig. S4b)† consists of three XPS peaks at 285.8, 286.0, 288.0 eV assigning to C–C, C–N, C–C═O groups of 6-aminohexanoic acid molecules, respectively.[45]

To understand the nature of the interaction between 6-aminohexanoic acid molecule and $MnWO_4$ nanoparticle surface, an experiment was carried out under the same reaction conditions for the synthesis of $MnWO_4$ nanoparticles, except for using hexamethylenediamine (two amino head-groups at the two ends of the molecule) instead of 6-aminohexanoic acid. $MnWO_4$ nanobars were obtained almost the same shape of the product prepared using 6-aminohexanoic acid (ESI, Fig. S5).† FTIR spectrum (ESI, Fig. S6)† of hexamethylenediamine-capped $MnWO_4$ nanobars shows the bands at 2920–2845 cm^{-1} are assigned to the C–H stretching modes of alkyl chain in hexamethylenediamine. The bands at 1458 and 3330 cm^{-1} are attributed to the C–N and N–H stretching modes of amino groups in hexamethylenediamine capping on $MnWO_4$ surface, respectively.[46] The bands at 600–830 cm^{-1} corresponding to the WO_4^{2-} vibrations are characteristic of $MnWO_4$.[47] It suggests that in order to keep the same shape of nanobar in both cases ($MnWO_4$ nanobars prepared using capping 6-aminohexanoic acid and hexamethylenediamine), the amino ($–NH_2$) functional groups capped on the nanobar surface possibly due to the predominant donor of their free electron pair. This is further illustrated by the FTIR spectra of free 6-aminohexanoic acid and 6-aminohexanoic acid-stabilized $MnWO_4$ sample (see below).

In this synthesis approach, water is adopted as the continuous solution phase and inorganic salts were used as starting materials. Due to the high solubility of the salts in aqueous solution, we could be applicable to synthesize the nanoparticles in scale up by using the high precursor monomer concentrations. This aqueous-based method is thus a promising way in the academic laboratory as well as can be expanded to the industrial scale in a simple way. The effect of precursor monomer concentration on the critical shape of the $MnWO_4$ nanobars for the large-scale synthesis was studied. The synthesis experiments were performed with different precursor (Mn + W) monomer concentrations from medium to high; from 0.122 to 0.305 M, and keeping other synthesis conditions unchanged (AHA/(Mn + W) molar ratio = 2 : 1, pH = 9, 180 °C, 20 h). Interestingly, as increasing the precursor monomer concentration from 0.122 to 0.305 M, the shape of the final product was not affected (nanobars with the aspect ratio of ~2.5), as shown in Fig. 6a and Fig. S7.† This may refer that the thermodynamically stability of the nanobars is established in a wide range of precursor monomer concentration (0.015–0.305 M). In fact, we obtained as much as 16 g of ~25 nm × 50 nm $MnWO_4$ nanobars per single run in a 700 mL-sized autoclave when the high precursor concentration of 0.122 M was used (Fig. 6). A schematic illustration for the formation and shape control of the products under different synthetic conditions can be overall summarized in details in Scheme 1.

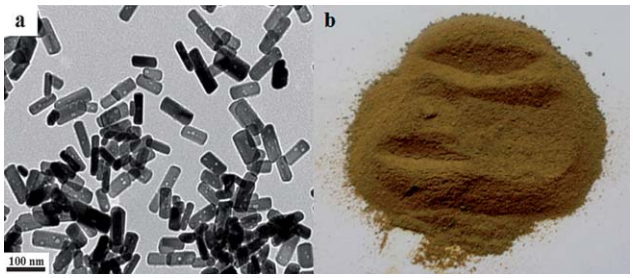

Fig. 6 (a) Typical TEM image of 25 nm × 50 nm $MnWO_4$ nanobars and (b) one photograph of ~16 g of 6-aminohexanoic acid-capped $MnWO_4$ nanobar powders synthesized using $[Mn^{2+}] = [WO_4^{2-}]$ of 0.122 M, 0.243 M of AHA, pH = 9, 180 °C for 20 h, in a 700 mL-sized autoclave.

Sacrificial organic surfactants can act as structure-directing agents or soft templates and are widely used to design nano/microstructures with peculiar morphologies.[48] For example, with the use of amino acid molecules, a variety of three-dimensional complex microarchitectures has been constructed.[49] In this work, we also found that the formation of 3D hierarchical $MnWO_4$ microspheres from the spontaneous assembly of primary $MnWO_4$ nanoparticles is very sensitive with low monomer precursor concentrations in the synthesis solution (*e.g.*, 0.0120–0.0076 M) of Mn^{2+} cation and WO_4^{2-} anion precursors, in the presence of 6-aminohexanoic acid surfactant. A series of experiments was carried out at the gradual decreased precursor concentration from 0.015 to 0.012, 0.0076 M, corresponding to the (Mn + W)/AHA molar ratio of 0.48 : 1, 0.39 : 1, 0.25 : 1, while keeping other reaction conditions unchanged ($[Mn^{2+}] = [WO_4^{2-}] = 1 : 1$, 0.031 M of AHA, pH = 9, 180 °C, 20 h). The morphologies and microstructures of the final products examined by SEM, TEM, SAED, XRD are shown in Fig. 7 and 10.

It is important to note that with the precursor monomer concentration of 0.015 M, only monodisperse single-crystalline nanobars with an average dimension of 25 nm × 50 nm were formed, and no nanobar aggregation was observed (see Fig. 1a). When the (Mn + W)/AHA molar ratio decreased from 0.48 : 1 to 0.39 : 1 (reducing 1.27 times of the precursor concentration in the initial solution), 25 nm × 50 nm-sized nanobars were intact. Polydisperse $MnWO_4$ microspheres with an average diameter of ~7 μm were however self-assembled from primary nanobars. Some nanobar stacks and individual nanobars were still observed at this precursor concentration (ESI, Fig. S8a–d).† It is worth pointing that when the (Mn + W)/AHA molar ratio decreased to 0.25 : 1 (reducing 2 times), the shape of the $MnWO_4$ nanobars (~25 nm × 50 nm) was still unchanged. These individual nanobars however had a greater tendency to form quite monodisperse hierarchical microspheres were formed, which are constituted from randomly individual nanorods. Fig. 7 shows SEM images of this product. The overall morphology of the $MnWO_4$ microsphere sample shows in Fig. 7a indicating that numerous microspheres with quite monodispersity with two size populations, 3–5 μm and 8–16 μm were achieved with this precursor concentration. Fig. 7b shows a single $MnWO_4$ microsphere with a diameter of 16 μm. As seen in Fig. 7c, the peripheral surface of the microsphere is rough and each microsphere is composed of numerous disordered nanobars suggesting that the formation of microspheres is likely driven by the interaction of inter-nanobars.

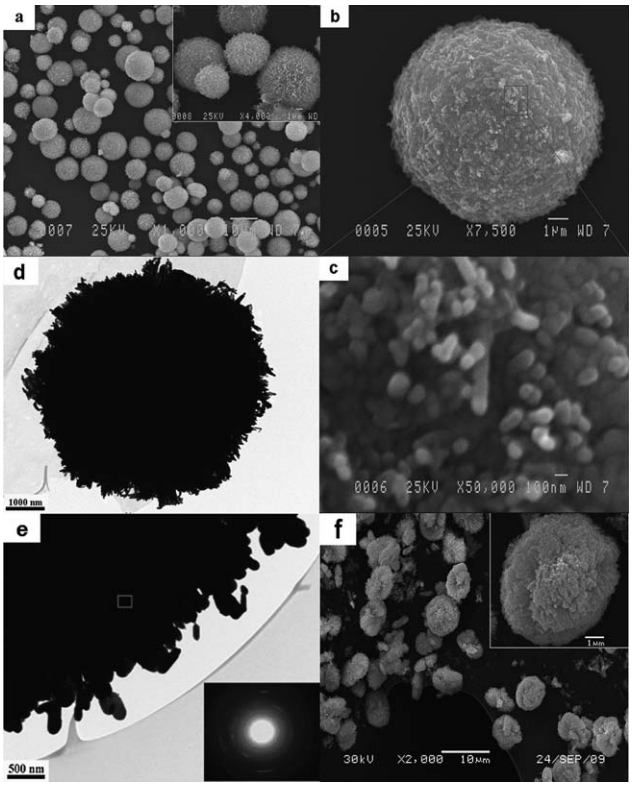

Fig. 7 Different-magnification SEM (a–c) and TEM (d and e) images, inset SAED pattern of the self-assembled $MnWO_4$ hierarchical microspheres synthesized using $[Mn^{2+}] = [WO_4^{2-}]$ of 0.0076 M, 0.0305 M of AHA, pH = 9, 180 °C for 20 h. (f) SEM image of the broken $MnWO_4$ microspheres achieving ultrasonic treatment. Furthermore, when water–ethylene glycol (10 : 30 mL) medium was used instead of 100% distilled water under the same synthetic conditions ($[Mn^{2+}] = [WO_4^{2-}] = 0.0076$ M, 0.031 M of AHA, pH = 9, 180 °C, 20 h) for the synthesis of $MnWO_4$ hierarchical microspheres (sample 8 in Table 1). The morphology and crystalline structure of the products are shown in Fig. 8.

This observation was further confirmed by TEM measurements. Fig. 7d displays a single $MnWO_4$ microsphere with an average diameter of 16 μm. Higher-magnification TEM image (Fig. 7e) taken at a border of this microsphere also exhibits the self-assembly of individual ~25 nm × 50 nm $MnWO_4$ nanobars, in good agreement with SEM observation. These nanobars were arranged disorderly instead of regularly on the surface. SAED pattern taken from a selected microsphere shows diffuse rings (inset Fig. 7e), indicating that the microsphere is polycrystalline, because it is composed of numerous primary nanobars. To obtain information about the inner structure of the hierarchical microspheres, $MnWO_4$ microspheres were cracked by ultrasonic treatment in a water batch for 30 min. As seen in Fig. 7f, their inner structure consists of nanobar blocks. It can be concluded that the formation of self-assembled $MnWO_4$ hierarchical microspheres from nanobars is favorable at relatively low precursor concentration (0.0076 M) of Mn^{2+} cation and WO_4^{2-} anion precursors in the initial synthesis solution.

Novel 3 μm-sized nanoplatelet-based microapples with two holes on their poles were observed (Fig. 8a–c). Fig. 8d presents TEM image of the $MnWO_4$ microapples with the same size. The whole microapple surface is composed of densely packed

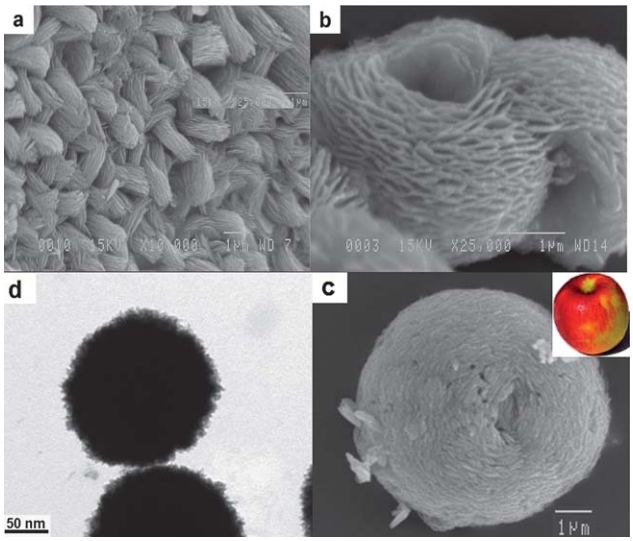

Fig. 8 Different-magnification SEM (a–c) and TEM (d) images of the nanoplatelet-based $MnWO_4$ micro-like apples synthesized in water–ethylene glycol medium (10 : 30 mL), $[Mn^{2+}] = [WO_4^{2-}]$ of 0.0076 M, 0.0305 M of AHA, at 180 °C for 20 h.

nanoplatelets aligned forming the apple-like structure. The nanoplatelets with an average thick of 15 nm are arranged regularly but not connected to each other. The formation of small nanoplatelets seems to be caused by the slow growth of $MnWO_4$ nuclei in the high viscous environment of ethylene glycol solvent. The porosity of the $MnWO_4$ hierarchical microspheres (sample 9 in Table 1) was generated by a removal of 6-aminohexanoic acid molecules upon calcination at 550 °C for 2 h.

SEM/TEM images of this calcined sample are shown in Fig. 9 indicating that the microspherical morphology was well remained even after calcination. XRD patterns of the as-made microspheres, as-made microapples, calcined microspheres of $MnWO_4$ (Fig. 10a–c) also show a pure monoclinic structure similar to the crystalline phase of the $MnWO_4$ nanobars. The broadening diffraction peaks also indicate that the $MnWO_4$ microspheres are composed of nanobars. Fig. 11a shows thermogravimetric analysis (TGA) curve of 6-aminohaxanoic acid-capped $MnWO_4$ microspheres (sample 9), from which only one weight-loss step (~24%) was observed. This step is in the range of 135 to 450 °C, corresponding to combustion and elimination of

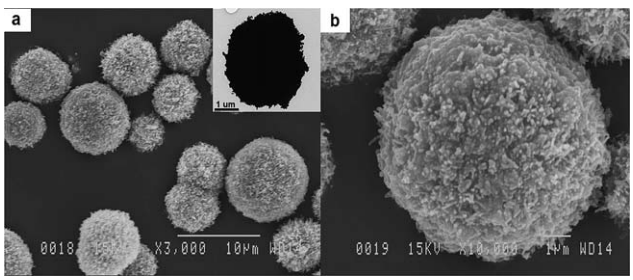

Fig. 9 Different-magnification SEM and inset TEM images of the as-synthesized $MnWO_4$ microspheres (sample 9 in Table 1) after calcination at 550 °C for 2 h.

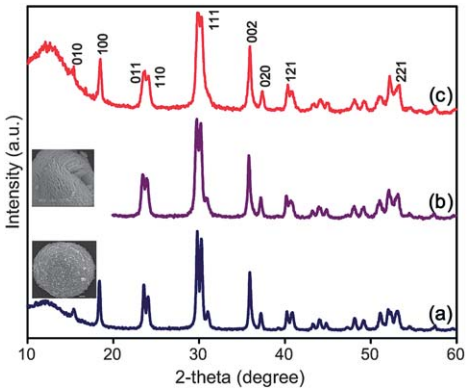

Fig. 10 XRD patterns of the $MnWO_4$ microstructure samples: (a) as-made microspheres (sample 9); (b) as-made micro-like apples (sample 10 in Table 1); (c) calcined microspheres.

6-aminohexanoic acid molecules. N_2 adsorption–desorption isotherms (Fig. 11b) of this calcined $MnWO_4$ microspheres exhibit a typical type-IV isotherm with a hysteretic loop in the range of 0.6–1.0 P/P_o, indicating the presence of mesoporosity in this material.[50] BET surface area, pore volume, BJH pore radius of this sample are ~30 m^2g^{-1}, ~0.38 cm^3g^{-1}, ~26 nm, respectively. The generated mesoporosity in this calcined material is owing to the inter-nanobar spaces, and a large mesopore size distribution could be due to a disordered aggregation of single-crystalline $MnWO_4$ nanoparticles. This clearly illustrates the formation of the mesocrystal microspheres.[51,52] Both the mesocrystal microspheres and micro-like apples are expected to have

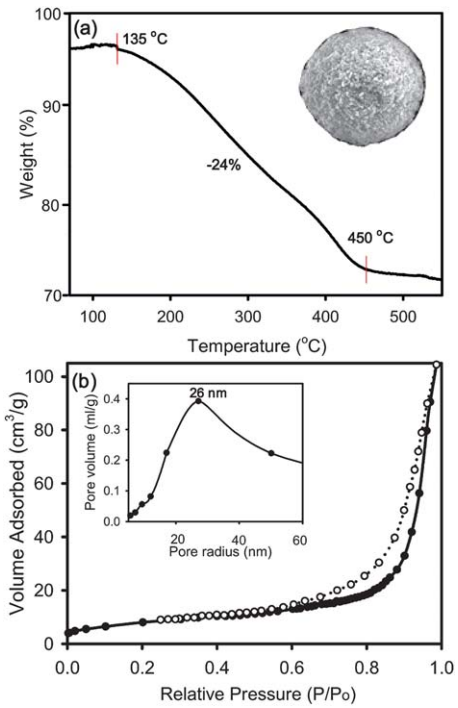

Fig. 11 (a) TGA curve of AHA-capped $MnWO_4$ microspheres (sample 9 in Table 1), inset SEM image of calcined microspheres and (b) nitrogen adsorption (filled symbols) and desorption (open symbols) isotherms and inset BJH pore radius distribution of the calcined $MnWO_4$ microspheres.

potential applications as many functional materials and reduced resistance to diffusion for adsorption and reaction, particularly, for large molecular guest species.

The formation of the $MnWO_4$ microspheres at the low monomer Mn/W precursor concentration could be associated with the peptide process of the carboxylic and amino groups of neighbouring 6-aminohexanoic acid molecules in aqueous solution to form dipeptide and/or polypeptide chains.[53] They can serve as polymer template like polyvinyl pyrrolidone (PVP),[54] to assemble nanoparticles yielding a second structure of $MnWO_4$ microspheres through the hydrogen-bonding interaction of polypeptides.[55]

To clarify the assembly mechanism of microspheres, FTIR spectra of free 6-aminohexanoic acid (AHA) and AHA-capped $MnWO_4$ microspheres (sample 9 in Table 1) were measured to assess the interaction between 6-aminohexanoic acid and nanobars, as well as the formation of peptide bonds. Fig. S9† indicates that FTIR bands at 2855–2950 cm^{-1} are attributed to the C–H stretching vibrations of methylene groups of the AHA molecule for both samples.[56] A band at 1386 cm^{-1} corresponding to C–N stretching mode of AHA molecules was identified in the both samples, which illustrated the binding of amino groups to the $MnWO_4$ nanobar surface.[57] The spectrum for free AHA shows two peaks at 1536 and 1560 cm^{-1} corresponding to the symmetric and asymmetric stretching vibrations of uncoordinated $–COO^–$ terminus of free AHA. For the AHA-capped $MnWO_4$ microsphere sample, the IR bands at 1536 and 1560 cm^{-1} were absent, however, an IR band at 1631 cm^{-1} corresponding to the stretching frequency of the C=O groups from peptide bonds (O=C···N–H) was observed.[58] Furthermore, a specific peak at 1160 cm^{-1} appeared corresponding to the stretching vibration of the peptide backbone.[59] These results prove that only the amino ($–NH_2$) group of AHA molecules capped on the surface of $MnWO_4$ nanoparticles and the free carboxylic (–COOH) terminus was oriented outward. The polypeptide chains were formed through the interaction between this uncoordinated carboxylic group on the nanobar surface and the amino group of residual 6-aminohexanoic acid in aqueous solution. These demonstrations indicate that the concentration of formed peptide chains in bulk solution is a critical factor during the self-assembly of the peptide structure and consequently affects the morphology and the formation of assembled $MnWO_4$ microspheres. The microsphere morphology can thus be controlled by adjusting the concentration of the peptide, that is, the concentration of 6-aminohexanoic acid.

This phenomenon can be considered that with a low concentration of Mn^{2+} and WO_4^{2-} precursors (0.0076 M, (Mn + W)/AHA molar ratio of 0.25 : 1), consequently, a low nucleation of $MnWO_4$ atoms, and a small amount of $MnWO_4$ nanoparticles was produced.[60,61] Due to the relatively high surfactant concentration (0.031 M), an excess amount of free 6-aminohexanoic acid exists in the aqueous synthesis solution, the dipeptide/polypeptide process of both $–NH_2$ and –COOH groups of free 6-aminohexanoic acid occurred on the basis of nucleophile mechanism,[62] resulting in the formation of polypeptide chains (polymer template). Because only small amount of $MnWO_4$ nanobars was yielded in bulk solution and the high AHA concentration, the peptide reaction continued and the reaction between the amino groups of the formed amino acid sequence of

protein (see ESI, Fig. S10)† and the uncoordinated carboxylic groups on the nanoparticle surface to generate the polypeptide-stabilized $MnWO_4$ nanobars. Subsequently, highly oriented backbone-backbone intermolecular hydrogen-bonding interactions of numerous amphiphilic polypeptide chains *via* either antiparallel or parallel arrangements were proceeded to spontaneous-assemble into polypeptide-stabilized $MnWO_4$ microspheres. These interactions are thermodynamically favorable due to the reduction of the particle surface energy when the interface is eliminated. On the contrary, a large amount of monodisperse nanobars was yielded using a higher precursor monomer concentration (0.015 M, (Mn + W)/AHA molar ratio of 0.48 : 1) with a faster nucleation of $MnWO_4$ atoms. The excess amount of free 6-aminohexanoic acid in synthesis solution decreased strongly because they were consumed more for the capping on nanobar surface. We believe that, herein, the construction of self-assembled microspheres can be confined because the dipeptide or/and polypeptide process of residual 6-aminohexanoic acid on the particle surface occurred in very low degree. A possible proposed mechanism of the "one-step" formation of self-assembled $MnWO_4$ hierarchical microspheres is illustrated in Scheme 2.

Fig. 12 shows UV-vis absorption and photoluminescence (PL) spectra of the sample 1: 25 nm × 50 nm $MnWO_4$ nanobar and sample 9: 7 μm $MnWO_4$ microspheres in Table 1. It is commonly accepted that the optical properties of the metal tungstate materials are strongly dependent on their morphology and crystallinity. Changes in shape would modify the electronic structures of tungstate leading to change in optical properties.[63] The UV-vis absorption spectra (Fig. 12A) of both nanobars and microspheres exhibit a single absorption peak at 284 nm, attributing to a charge-transfer transition between the O 2p orbitals and the empty d orbitals of the central W ion.[64] The broadening absorption of the nanobars could result of the smaller particle size of products owing to quantum confinement effect.[65] The PL emission spectra (Fig. 12B) of these samples show the same blue emission bands at 449, 483, 527, 559 nm under the 253 nm excitation. These emission bands are attributed to the transition from the $^1A_1$ ground-state to the high vibration level of $^1T_2$ and from the low vibration level of $^1T_2$ to the $^1A_1$ ground-state within the tetragonal WO_4^{2-} groups.[21] This is due to the excitation of WO_4^{2-} group from charge-transfer p–d transition. As a result, the emission band positions are not strongly dependent on the morphology of the $MnWO_4$ lattices. However, using the same particle concentration under the identical measurement conditions, the nanobars show a higher up conversion efficiency than that the microspheres. The relative intensity of the nanobars is almost 2.5 times higher than that of the microspheres. Because the size of nanobars (~25 nm × 50 nm) is almost the same for the both samples, a lower PL emission intensity of the $MnWO_4$ microspheres compared to that of the $MnWO_4$ nanobars could be due to a part of nanobars inside of microspheres. It also indicates that an exposed surface of the microspheres under the excitation is lower than that of nanobars.

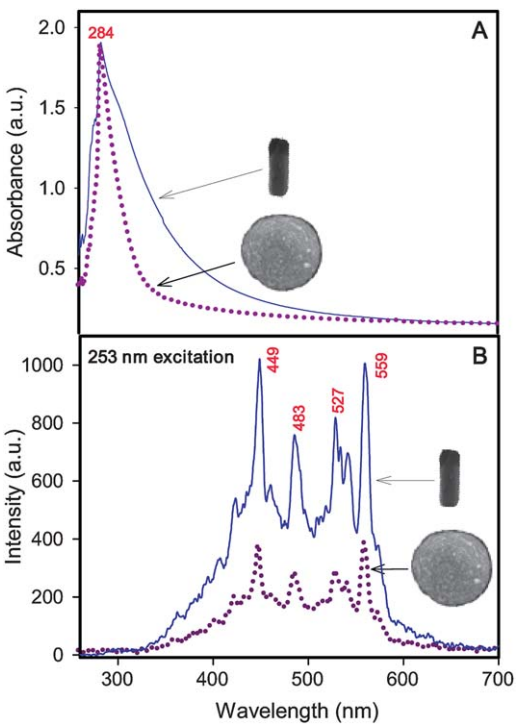

Fig. 12 (A) UV-vis absorption and (B) photoluminescence emission spectra of 25 nm × 50 nm $MnWO_4$ nanobars (sample 1) and 7 μm $MnWO_4$ microspheres (sample 9 in Table 1).

4. Conclusions

In conclusion, we have developed a facile single-step approach for the large-scale synthesis of the single-crystalline $MnWO_4$ nanoparticles and 3D hierarchical mesocrystal microspheres from the hydrothermal reaction in water or water/ethylene glycol medium using $Mn(NO_3)_2$ and Na_2WO_4, as starting precursors and capping bifunctional amino acid biomolecules with different alkyl chain lengths such as 5-aminovaleric acid, 6-aminohexanoic acid, 2-aminononanoic acid. Monodisperse $MnWO_4$ nanoparticles were capped by the amino head group of amino acid biomolecules and the uncoordinated carboxylic terminus were oriented outward to provide the water-dispersible nature of the hydrophilic nanoparticles. The uniform single-crystalline $MnWO_4$ nanoparticles with bar, rod, square, quasi-sphere, sphere, hexagonal shapes were achieved by tuning the synthesis parameters such as the concentration and the alkyl chain length of amino acids, pH of solution, and reaction temperature. Furthermore, by decreasing the Mn^{2+} and WO_4^{2-} precursor monomer concentration from 0.0150 to 0.0076 M in water medium, rigid $MnWO_4$ mesocrystal hierarchical microspheres were formed from the spontaneous-assembly of primary nanoparticles through the backbone-backbone intermolecular hydrogen-bonding interactions of polypeptide chains. Using water/ethylene glycol (10 : 30 mL) instead of distilled water medium, novel nanoplatelet-based microapples with two holes on their poles were yielded. The mesocrystal microspheres with relatively high porosity were generated after removal of surfactant upon calcination.

The photoluminescence results indicate that the PL emission intensity of the $MnWO_4$ nanobars is higher than that of the $MnWO_4$ microspheres indicating the decrease in the luminescence efficiency of the microspheres due to nanobars inside of

microspheres. This current approach is easy to scale up (for example, uniform $MnWO_4$ nanobars can be produced in a large quantity of ~16 g in a single preparation run), using inexpensive precursors, amino acid biomolecules as bifunctional surfactant, water as environmentally solvent. We believe that these shape-controlled $MnWO_4$ nanoparticles and 3D hierarchical $MnWO_4$ mesocrystal microspheres have highly potential applications in photocatalysis, humidity sensor, *etc.* The synthetic procedure can be extended to the "green" synthesis of other nanomaterials.

Acknowledgements

This work was supported by the Natural Sciences and Engineering Research Council of Canada (NSERC) through a strategic grant.

References

1 U. Banin, *Nat. Mater.*, 2007, **6**, 625.
2 Z. Nie, A. Petukhova1 and E. Kumacheva1, *Nat. Nanotechnol.*, 2010, **5**, 15.
3 A. V. Blaaderen, *Nature*, 2009, **461**, 892.
4 C. B. Burda, X. B. Chen, R. Narayanan and M. A. E. Sayed, *Chem. Rev.*, 2005, **105**, 1025.
5 H. G. Yang, C. H. Sun, S. Z. Qiao, J. Zou, G. Liu, S. C. Smith, H. M. Cheng and G. Q. Lu, *Nature*, 2008, **453**, 638.
6 X. W. Lou, L. A. Archer and Z. Yang, *Adv. Mater.*, 2008, **20**, 3987.
7 S. C. Glotzer and M. J. Solomon, *Nat. Mater.*, 2007, **6**, 557.
8 W. Fan, M. A. Synder, S. Kumar, P. S. Lee, W. C. Yoo, A. V. Mccormick, R. L. Penn, A. Stein and M. Tsapatsis, *Nat. Mater.*, 2008, **7**, 984.
9 J. Zhuang, A. D. Shaller, J. Lynch, H. Wu, O. Chen, A. D. Q. Li, Y. C. Cao and J. Am, *J. Am. Chem. Soc.*, 2009, **131**, 6084.
10 W. M. Qu, W. Wlodarski and J. U. Meyer, *Sens. Actuators, B*, 2000, **64**, 76.
11 A. H. Arkenbout, T. T. M. Palstra, T. Siegrist and T. Kimura, *Phys. Rev. B: Condens. Matter Mater. Phys.*, 2006, **74**, 184431.
12 O. Heyer, N. Hollmann, I. Klassen, S. Jodlauk, L. Bohaty, P. Becker, J. A. Mydosh, T. Lorenz and D. Khomskii, *J. Phys.: Condens. Matter*, 2006, **18**, L471.
13 K. Taniguchi, N. Abe, T. Takenobu, Y. Iwasa and T. Arima, *Phys. Rev. Lett.*, 2006, **97**, 097203.
14 Y. Xing, S. Song, J. Feng, Y. Lei, M. Li and H. Zhang, *Solid State Sci.*, 2008, **10**, 1299.
15 L. Zhang, C. Lu, Y. Wang and Y. Cheng, *Mater. Chem. Phys.*, 2007, **103**, 433.
16 W. Qu, W. Wlodarski and J. U. Meyer, *Sens. Actuators, B*, 2000, **64**, 76.
17 R. Bharat and R. A. Singh, *J. Phys. Chem. Solids*, 1982, **43**, 641.
18 M. A. K. L. Dissanayake, P. A. R. D. Jayathilaka and R. S. P. Bokalawela, *Electrochim. Acta*, 2005.
19 Y. X. Zhou, Q. Zhang, J. Y. Gong and S. H. Yu, *J. Phys. Chem. C*, 2008, **112**, 13383.
20 L. Zhang, C. Lu, Y. Wang and Y. Cheng, *Mater. Chem. Phys.*, 2007, **103**, 433.
21 F. Zhang, Y. Yiu, M. C. Aronson and S. S. Wong, *J. Phys. Chem. C*, 2008, **112**, 14816.
22 S. H. Yu, B. Liu, M. S. Mo, J. H. Huang, X. M. Liu and Y. T. Qian, *Adv. Funct. Mater.*, 2003, **13**, 639.
23 S. Thongtem, S. Wannapop, A. Phuruangrat and T. Thongtem, *Mater. Lett.*, 2009, **63**, 833.
24 Y. X. Zhou, Q. Zhang, J. Y. Gong and S. H. Yu, *J. Phys. Chem. C*, 2008, **112**, 13383.
25 D. Mrabet, M. H. Zahedi-Niaki and T. O. Do, *J. Phys. Chem. C*, 2008, **112**, 7124.
26 T. D. Nguyen, D. T. Cao, T. N. Dinh and T. O. Do, *J. Phys. Chem. C*, 2009, **113**, 18584.
27 T. D. Nguyen, C. T. Dinh and T. D. Do, *Langmuir*, 2009, **25**, 11142.
28 C. T. Dinh, T. D. Nguyen, F. Kleitz and T. O. Do, *ACS Nano*, 2009, **3**, 3737.
29 T. D. Nguyen, C. T. Dinh and T. O. Do, *ACS Nano*, 2010, **4**, 2263–2273.
30 D. Wang, T. Xie, Q. Peng and Y. Li, *J. Am. Chem. Soc.*, 2008, **130**, 4016.
31 E. E. Lees, T. L. Nguyen, A. H. A. Clayton and P. Mulvaney, *ACS Nano*, 2009, **3**, 1121.
32 B. Liu, H. C. Zeng and J. Am, *J. Am. Chem. Soc.*, 2004, **126**, 8124.
33 W. S. Wang, L. Zhen, C. Y. Xu, B. Y. Zhang and W. Z. Shao, *J. Phys. Chem. B*, 2006, **110**, 23154.
34 S. Lei, K. Tang, Z. Fang, Y. Huang and H. Zheng, *Nanotechnology*, 2005, **16**, 2407.
35 R. L. Penn and J. Phys, *J. Phys. Chem. B*, 2004, **108**, 12707.
36 J. W. Mullin, *Crystallization*, 3rd ed; Butterworth-Heinemann: Woburn, MA, 1997.
37 G. Wulff and F. Zeitschrift, *Beitr. Krystallogr. Mineral.*, 1901, **34**, 449.
38 Y. Yin and A. P. Alivisatos, *Nature*, 2005, **437**, 664.
39 Joint Committee on Powder Diffraction Standards diffraction data file no. 13–434, *International Center for Diffraction Data*, Newtown Square, PA, USA, 1963.
40 T. D. Nguyen and T. O. Do, *Langmuir*, 2009, **25**, 5322.
41 J. F. Moulder, W. F. Stickle, P. E. Sobol, K. D. Bomben, *Handbook of X-ray photoelectron spectroscopy*; Perkin-Elmer corporation, Physical Electronics Division, 1992.
42 F. Zhang, M. Y. Sfeir, J. A. Misewich and S. S. Wong, *Chem. Mater.*, 2008, **20**, 5500.
43 Q. Zhang, X. Chen, Y. Zhou, G. Zhang and S. H. Yu, *J. Phys. Chem. C*, 2007, **111**, 3927.
44 V. V. Atuchin, V. G. Kesler, N. Y. Maklakova, L. D. Pokrovsky and D. V. Sheglov, *Eur. Phys. J. B*, 2006, **51**, 293.
45 Z. Deng, B. Peng, D. Chen, F. Tang and A. Muscat, *Langmuir*, 2008, **24**, 11089.
46 J. Yang and J. Y. Ying, *Nat. Mater.*, 2009, **8**, 683.
47 Y. X. Zhou, Q. Zhang, J. Y. Gong and S. H. Yu, *J. Phys. Chem. C*, 2008, **112**, 13383.
48 B. L. Cushing, V. L. Kolesnichenko and C. J. O'Connor, *Chem. Rev.*, 2004, **104**, 3893.
49 F. C. Meldrum and H. Colfen, *Chem. Rev.*, 2008, **108**, 4332.
50 Y. Li, M. Cao and L. Feng, *Langmuir*, 2009, **25**, 1705.
51 A. N. Kulak, P. Iddon, Y. Li, S. P. Armes, H. Colfen, O. Paris, R. M. Wilson and F. C. Meldrum, *J. Am. Chem. Soc.*, 2007, **129**, 3729.
52 R. Q. Song and H. Colfen, *Adv. Mater.*, 2010, **22**, 1301.
53 J. D. Hartgerink, E. Beniash and S. I. SStupp, *Science*, 2001, **294**, 1684.
54 M. H. Kim, B. Lim, E. P. Lee and Y. Xia, *J. Mater. Chem.*, 2008, **18**, 4069.
55 S. Kiyonaka, K. Sada, I. Yoshimura, S. Shinkai, N. Kato and I. Hamachi, *Nat. Mater.*, 2004, **3**, 58.
56 T. D. Nguyen, D. Mrabet and T. D. Do, *J. Phys. Chem. C*, 2008, **112**, 15226.
57 L. Polavarapu and Q. H. Xu, *Nanotechnology*, 2008, **19**, 075601.
58 N. T. Whilton, P. J. Vickers and S. Mann, *J. Mater. Chem.*, 1997, **7**, 1623.
59 Z. Zhang, D. Gao, H. Zhao, C. Xie, G. Guan, D. Wang and S. H. Yu, *J. Phys. Chem. B*, 2006, **110**, 8613.
60 R. Xie, Z. Li, X. Peng and J. Am, *J. Am. Chem. Soc.*, 2009, **131**, 15457.
61 S. G. Kwon, Y. Piao, J. Park, S. Angappane, Y. Jo, N. M. Hwang, J. G. Park, T. Hyeon and J. Am, *J. Am. Chem. Soc.*, 2007, **129**, 12571–12584.
62 H. Matsui, B. Gologan, H. Schaffer, F. Adar, D. Seconi and O. Phanstiel, *Langmuir*, 2000, **16**, 3148.
63 L. Xu, J. Shen, C. Lu, Y. Chen and W. Hou, *Cryst. Growth Des.*, 2009, **9**, 3129.
64 Q. Zhang, X. Chen, Y. Zhou, G. Zhang and S. H. Yu, *J. Phys. Chem. C*, 2007, **111**, 3927.
65 M. A. El-Sayed, *Acc. Chem. Res.*, 2004, **37**, 326.

